

16 Abstract

17 Throughout all oceans, aggregations of zooplankton and ichthyoplankton appear as horizontal
18 sound scattering layers (SSLs) when detected with active acoustic techniques. Quantifying the
19 composition and density of these layers is prone to sampling biases. We conducted a net and
20 trawl survey of the epipelagic fauna in northern Norway (70°N) in June 2018 while an
21 autonomous surface vehicle equipped with a broadband echosounder (283-383 kHz) surveyed
22 the same region. Densities from the autonomous hydroacoustic survey were calculated using
23 forward estimates from the relative density from the net and trawl, and inversion estimates
24 with statistical data-fitting. All four methods (net, trawl, acoustic forward and inverse methods)
25 identified that copepods dominated the epipelagic SSL, while pteropods, amphipods and fish
26 larvae were present in low densities. The density estimates calculated with the inverse method
27 were higher for mobile zooplankton, such as euphausiid larvae, than with the other methods.
28 We concluded that the inverse method applied to broadband autonomous acoustic surveys
29 can improve density estimates of epipelagic organisms by diminishing avoidance biases and
30 increasing the spatio-temporal resolution of ship-based surveys.

31

32 Keywords: broadband acoustics, inversion, machine learning, autonomous surface vehicle,
33 zooplankton

34 Introduction

35 Pelagic zooplankton and ichthyoplankton form dense horizontal aggregations throughout all
36 oceans and represent an easily accessible food source for higher trophic levels. In the North
37 Atlantic, these organisms funnel energy from primary producers to top predators such as
38 marine mammals, seabirds, and the pelagic early life stages of larger fishes targeted by
39 commercial fisheries, e.g., Atlantic cod (*Gadus morhua*) (Falk-Petersen and Hopkins, 1981;
40 Solvang et al. 2021). Accurate density estimates of zooplankton and ichthyoplankton are thus
41 needed to calculate and model energy transfer in marine environments.

42 The density of zooplankton and ichthyoplankton can be calculated for large volumes of water
43 using hydroacoustic surveys because the aggregations appear as sound scattering layers (SSLs)
44 when detected with echosounders (Dietz, 1948; Barham, 1966; Proud et al., 2018). At high
45 latitudes, for example in the Fram Strait, the backscatter from the SSLs is usually much stronger
46 in the epipelagic zone (< 200 m) than in the mesopelagic zone (> 200 m), suggesting that there
47 is a higher density of biomass near the surface than below 200 m (Knutsen et al., 2017;
48 Gjørseter et al., 2020). Epipelagic SSLs of zooplankton, mainly euphausiids, copepods,
49 amphipods, pteropods, and juvenile fish, have been detected with acoustics over high latitude
50 shelves (Knutsen et al., 2017, Bandara et al., 2022), in fjords in Northern Norway (Falk-Petersen
51 and Hopkins, 1981; Falk-Petersen and Kristiansen, 1985), and in deeper basins of the Barents
52 Sea (Gjørseter et al., 2020). However, density estimates of epipelagic organisms generally
53 contain several biases because of 1) the draft of research vessels and the near-field of acoustic
54 instruments which form a blind zone in the top ca. 10 m (e.g., Pedersen et al., 2019); 2)
55 variation in detection probability with density and range (Appenzeller and Leggett, 1992;
56 Demer and Hewitt, 1995; Simmonds and MacLennan, 2008); and 3) the sound and light

57 emitted by research vessels (Trevorrow et al., 2005; De Robertis et al., 2012; Peña, 2019; Berge
58 et al., 2020).

59 New technology can contribute to minimizing uncertainties in the detection and density
60 estimates of epipelagic organisms. The recent development of autonomous surface and
61 subsurface vehicles with compact and energy-efficient active acoustic systems reduces the
62 blind zone as well as artificial noise and light sources compared to traditional acoustic surveys
63 conducted from research vessels. These autonomous platforms also have the potential to
64 increase the temporal and spatial scale of acoustic surveys (e.g., Mordy et al., 2017; De Robertis
65 et al., 2019; Verfuss et al., 2019). Concomitantly, the development of broadband echosounders
66 (Andersen et al., 2021) and scattering models for several taxonomic groups (Jech et al., 2015)
67 have improved our ability to detect and characterise small (<1 cm) acoustic targets at a high
68 vertical resolution.

69 Two methods can be used to estimate density from the acoustic signal scattered from dense
70 epipelagic aggregations of zooplankton and ichthyoplankton in SSLs: the forward method and
71 the inverse method. The forward method uses the relative density of each taxonomic group
72 based on net and trawl samples from the survey region to allocate a proportion of the
73 backscatter, the sound intensity reflected by the targets, for a density estimate of each
74 taxonomic group (Love, 1975; Simmonds and MacLennan, 2008). However, each net or trawl
75 is inherently selective (Skjoldal et al., 2013) depending on mesh size, net/trawl opening, tow
76 speed, and species density (Pearcy et al., 1983; Battaglia et al., 2006; Moriarty et al., 2018).
77 Ultimately, with the forward method, biases from net and trawl selectivity are transferred to
78 the species density estimates. The inverse method rather directly calculates the density of each
79 taxonomic group from acoustic data by optimising the densities based on the received

80 backscatter and the scattering models of each species (Holliday, 1977). When applying the
81 inverse method to broadband acoustics, the spectrum of the acoustic signal can be fully
82 exploited to optimize the model fitting and calculations of density for each taxonomic group.
83 Applying the inverse method to broadband acoustic data has the potential to reduce the bias
84 from net and trawl selectivity and could increase the value of datasets from autonomous or
85 remotely operated platforms with sparse net validation.

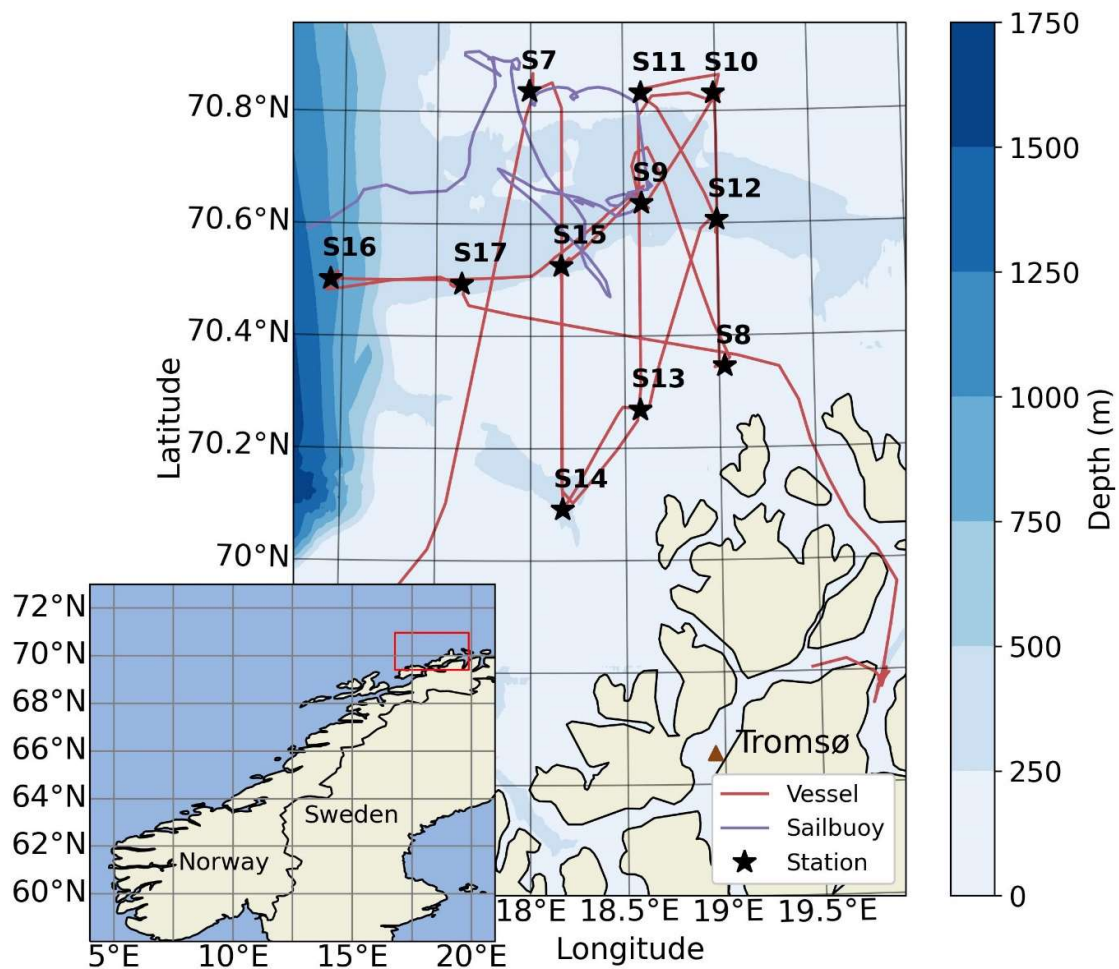
86 This study assessed zooplankton and ichthyoplankton density estimates in a near-surface SSL
87 using four different methods: mesozooplankton net (MultiNet), macrozooplankton trawl
88 (Tucker trawl), and the forward and inverse methods applied to broadband acoustic data
89 collected with an autonomous surface vehicle. The survey was conducted as a case study in
90 the Tromsøflaket area, a bank north of the northern Norwegian Sea (70° N). We deployed nets
91 and trawls from a research vessel while an autonomous surface vehicle equipped with a
92 broadband echosounder surveyed the same region (Camus et al., 2019). We also tested the
93 applicability of using theoretical scattering models (Chu and Ye, 1999; Khodabandeloo et al.,
94 2021) to reduce the dependence on relative density estimates from net and trawl sampling
95 when conducting autonomous hydroacoustic surveys. The limitations of each method are
96 discussed and we provide recommendations on combining sampling methods to increase the
97 accuracy of zooplankton and ichthyoplankton studies.

98 **Materials and methods**

99 **I. Study area and survey design**

100 Tromsøflaket is comprised of a plateau (150 – 250 m depth) located at the southwestern
101 entrance of the Barents Sea (Figure 1). The plateau is an area of high biological activity; some

102 bank areas are heavily trawled as they support a rich community of commercially harvested
103 fish (Olsen et al., 2010). It is a difficult region for traditional ecosystem sampling activity despite
104 the relatively shallow bank because of the strong and variable currents (Bellec et al., 2008;
105 Kędra et al., 2017).



106

107 Figure 1: Map of the Norwegian Sea and Norway's coasts. The red box in the inset indicates
108 the area shown in the large bathymetric map of Tromsøflaket. The Tromsøflaket map
109 indicates the vessel-based research cruise track in red as it travelled between sampling
110 stations (black stars). Time and GPS location of stations are described in Table 1, and Sailbuoy
111 track in purple is the autonomous acoustic survey. Map produced with cartopy (ver. 0.18.0;

112 scitools.org.uk/cartopy) in orthographic projection and the inset in plate carrée projection
113 (UTM coordinate system).

114 Tromsøflaket was surveyed from June 20th to 29th, 2018, from the R/V *Helmer Hanssen* and an
115 autonomous surface vehicle (Sailbuoy, Offshore Sensing, Bergen, Norway, www.sailbuoy.no).
116 During the R/V *Helmer Hanssen* cruise, environmental data and biological samples were
117 collected at 11 stations to estimate zooplankton and fish composition, density, and vertical
118 distribution (Stations 7 to 17; Table 1). The Sailbuoy was deployed from the vessel at Station 7
119 on June 21st. It was picked up from Station 11 on June 22nd to fix issues with the storage of
120 acoustic data and relaunched on June 24th at Station 9. The Sailbuoy left the study area on June
121 29th and was recovered south of Lofoten on August 22nd. The ship left the study area on June
122 25th. For this study, we only used the data from the Tromsøflaket region as delimited in Figure
123 1.

124 Table 1: The location and time of sampling stations within the Tromsøflaket region during the
125 SeaPatches research cruise with R/V *Helmer Hanssen*.

Station	Date	Time (UTC)	Latitude (°N)	Longitude (°E)
S7	21/06/2018	03:53:00	70.836	17.996
S8	22/06/2018	03:48:00	70.345	19.028
S9	22/06/2018	17:15:00	70.636	18.595
S10	23/06/2018	01:01:00	70.831	18.988
S11	23/06/2018	05:50:00	70.833	18.597
S12	23/06/2018	13:40:00	70.606	18.999
S13	23/06/2018	22:45:00	70.268	18.581
S14	24/06/2018	02:14:00	70.091	18.169

S15	24/06/2018	10:57:00	70.525	18.166
S16	25/06/2018	05:35:00	70.500	16.936
S17	25/06/2018	20:26:00	70.493	17.636

126

127 II. Biological sampling

128 Mesozooplankton were sampled by vertical hauls (towing speed 0.5 m s^{-1}) using a multiple
129 opening/closing net (MultiNet, Hydro-Bios, Kiel, Germany, www.hydrobios.de; mouth opening
130 0.25 m^2 , mesh size $180 \mu\text{m}$). Five depth strata (bottom-100, 100-30, 30-10, 10-5, and 5-0 m)
131 were sampled at each station, but data below 100 m were not used in this study because it
132 was outside the range of the echosounder mounted on the Sailbuoy. At station 13, samples
133 were taken by a ring net (WP2 net, Hydro-Bios), with the same mouth opening, mesh size and
134 depth strata as the MultiNet, but did not include the 0-5 m depth stratum. All samples were
135 preserved in 4% formaldehyde-in-seawater solution buffered with hexamine. Taxonomic
136 analyses were completed in the laboratory. Large organisms (total length $> 5 \text{ mm}$) were picked
137 out using forceps, identified, and counted from the whole sample. The remainder of the
138 sample was examined by sub-sampling with aliquots obtained with a 5 ml automatic pipette,
139 with the pipette tip cut at 5 mm diameter to allow a free collection of mesozooplankton. The
140 number of subsamples analysed was chosen so that at least 150 individuals of copepods
141 (*Calanus* spp.) and 300 other organisms were counted. To assess the length frequency
142 distribution of the *Calanus* population, the prosome length of all counted individuals of *Calanus*
143 spp. was measured from the tip of the cephalosome to the distal lateral end of the last thoracic
144 segment. In addition, body length of euphausiids, amphipods, pteropods, and fish larvae were
145 measured from subsamples of Multinet samples taken at stations 8 through 17. Body length
146 of euphausiids and amphipods was measured on stretched animals along the dorsal line from

147 the tip of the rostrum (euphausiids) or the anterior edge of the eye (amphipods) to the tip of
148 the telson. Body length of pteropods was measured as the diameter of their shell. Total length
149 of fish larvae was measure the most forward point of the head to the farthest tip of the tail
150 with the fish lying on its side. Zooplankton density (individuals per m³) was estimated for each
151 species by stratum by correcting for the mouth-opening area of the net and vertical hauling
152 distance of the statum, assuming 100% filtration efficiency. The weighted mean density
153 estimate for each species per station over the 0-100 m range was calculated using the following
154 equation:

$$155 \quad \rho = \frac{\sum_{i=1}^n \rho^i dz^i}{\sum_{i=1}^n dz^i},$$

156 *(Equation 1)*

157 where n is the number of strata, ρ^i is the density of the species in the stratum i in individuals
158 per m³ (ind. m⁻³) and dz^i is the thickness of each stratum i in meters.

159 Macrozooplankton and ichthyoplankton were sampled with a Tucker trawl (1 m² opening and
160 1000 μ m mesh size) towed for 15 minutes at 2 knots between 20 to 40 m depth. The targeted
161 depth at each station was determined from the epipelagic SSL identified in the echogram from
162 the vessel's echosounders (Kongsberg Maritime AS, Horten, Norway, www.kongsberg.com;
163 Simrad EK60, 18 and 38 kHz, 1.024 ms pulse duration, 2 Hz pulse repetition). All samples were
164 preserved in a 4% formaldehyde-in-seawater solution buffered with hexamine. Density
165 estimates from the Tucker trawl samples were analysed per station. Each station was sub-
166 sampled using a plankton splitter and counted until at least 300 individuals were identified.
167 The count of each species was extrapolated to the entire sample size and converted to density
168 by accounting for the mount-opening area, deployment speed and time. To document the

169 length distribution of dominant macrozooplankton species captured with the Tucker trawl,
170 random subsamples of euphausiids, amphipods, pteropods and fish larvae were taken from
171 samples of stations 7, 8 and 9 and body length was measured as described above.

172 For both MultiNet and Tucker trawl samples, species were grouped by taxon. Four taxonomic
173 groups were most abundant: copepods, euphausiid larvae, amphipods, and pteropods.
174 Additionally, fish larvae were included in the analysis because of the high sonar reflectivity of
175 their swimbladder and their socio-economic importance.

176 III. Acoustic sampling

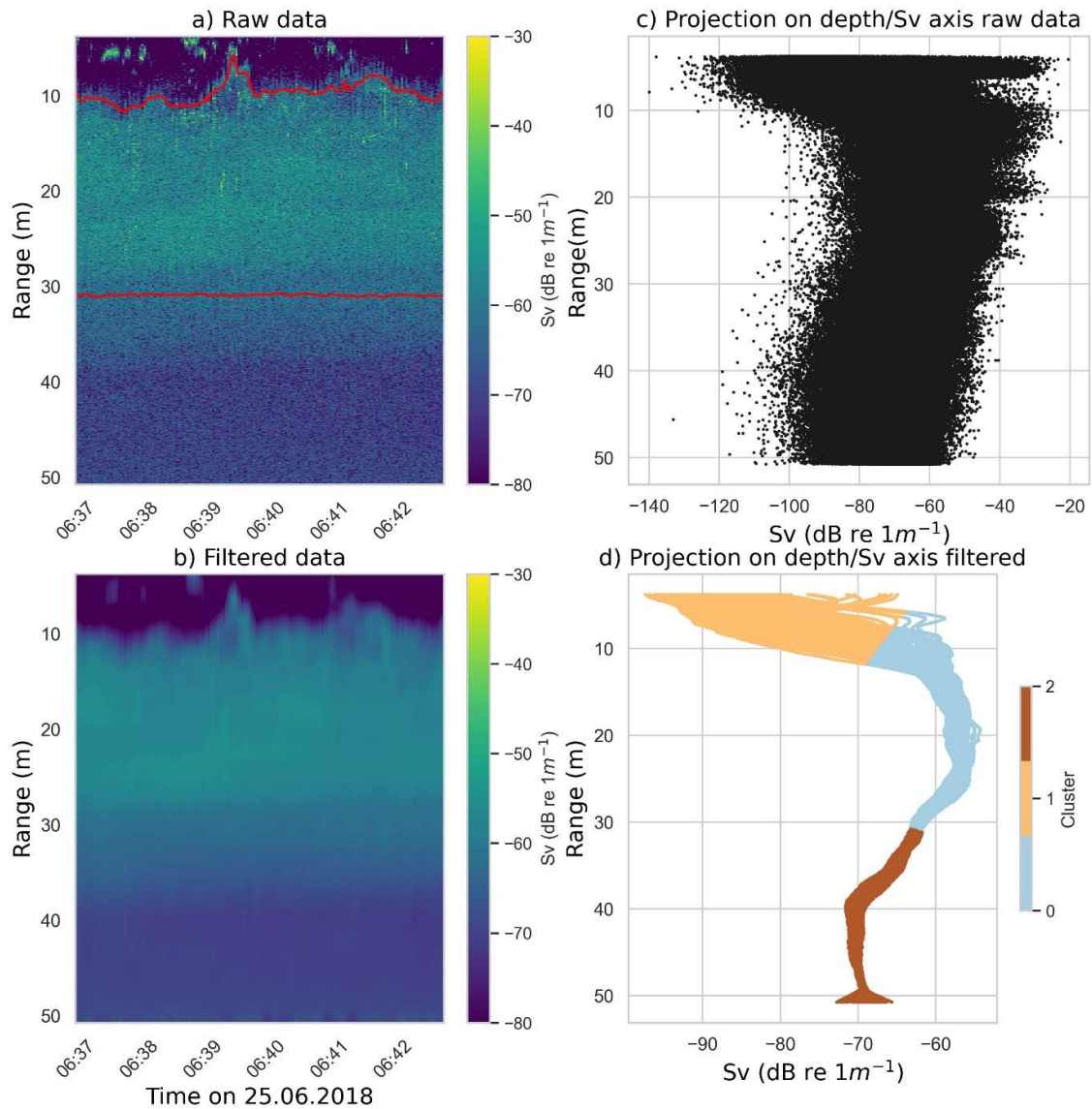
177 A. Acoustic data processing

178 The autonomous hydroacoustic survey was completed using a Sailbuoy equipped with a WBT
179 Mini (Kongsberg Maritime AS) with a 333 kHz transducer (ES333-7CDK split-beam) operating
180 in broadband mode (283-383 kHz, 1.024 ms pulse duration, 0.5 Hz pulse repetition, fast
181 ramping) for 5 minutes every half hour. The transducer was mounted on the bottom of the
182 Sailbuoy keel at 0.5 m depth. The Sailbuoy keel was always in the water and the transducer
183 was always submerged. Echosounder calibration was performed before the deployment and
184 after the retrieval with a 22.0 mm tungsten carbide (6% cobalt binding) calibration sphere
185 (Demer et al., 2015). Broadband calibration parameters were calculated with the EK80
186 calibration wizard (version 2.0.1, EK80 software, Kongsberg Maritime AS), and the parameter
187 values were linearly interpolated over the inhibition bands that covered the nulls. Data were
188 calibrated and processed in Echoview (version 12.1, Echoview Software Pty Ltd, Hobart,
189 Australia, www.echoview.com). The maximum range for the analysis was set to 50 m (50.5 m

190 depth) because the signal to background noise ratio diminished below 10 dB (for a signal of -
191 70 dB) at greater ranges.

192 B. Sound scattering layer backscatter spectra

193 Sound scattering layers forming discrete horizontal bands of backscatter above the background
194 noise (Proud et al., 2015) were identified using k-means clustering, an unsupervised machine
195 learning algorithm (Lloyd, 1982). Each raw data file output from the echosounder was
196 converted into a netCDF4 file with the open-source software echopype (version 0.5.3; Lee et
197 al., 2021; Figure 2a). Data analysis was restricted to the region between the near-field (3 m
198 range) and the signal-to-noise ratio limit (50 m range). In all echograms, a maximum of one SSL
199 was detected by the clustering algorithm in the upper 50.5 m of the water column. The SSL
200 varied in strength, thickness, and depth. The pulse-compressed volume backscattering
201 strength (S_v in dB re 1m^{-1}) averaged over the frequency spectrum was pre-processed with a
202 mean filter to smooth the backscatter in time (35 pings; or 70 s) and depth (15 bins; or 0.09 m)
203 (Figure 2b). The pre-processing filter revealed the SSL on the depth/ S_v projection, as shown in
204 the comparison between the unfiltered data in Figure 2c and the filtered data in Figure 2d.



205

206 Figure 2: Example of a) raw pulse-compressed volume backscattering strength (Sv) echogram

207 data upper and lower boundaries of Cluster 0 in red; b) echogram after the mean filtering in

208 time and depth (70 s and 0.09 m filter, respectively); c) projection of raw data by removing

209 the time dimension; and d) projection of filtered data in the depth/Sv dimensions classified

210 into clusters (k=3 in this example) obtained by k-means clustering. In this example, the cluster

211 corresponding to the SSL is Cluster 0.

212 After the pre-processing, we applied k-means clustering on the depth/ S_v dimensions of each
213 data file (between 3 to 5 minutes of data, depending on the file size). The k-means clustering
214 algorithm categorises all the data points into different groups (i.e., clusters). The only
215 parameter adjusted for each SSL was the number of clusters. The other k-means parameters
216 stayed the same for each iteration (k-mean++ initialisation, 10 separate runs, tolerance of $1e^{-4}$,
217 and a maximum of 300 iterations). Selecting the optimal number of clusters is an intrinsic
218 challenge with k-means clustering. Here, the number of clusters was optimal when the entire
219 SSL was grouped into one of the clusters. The SSLs were easier to delineate by clustering when
220 they were thick, had a high S_v and had a distinct separation from surface bubbles or entrained
221 air (Anderson et al., 2007). We typically selected between 3-7 clusters. For example, in Figure
222 2d where Cluster 0 corresponds to the SSL, we chose to separate the backscatter profile into
223 3 clusters because of the relatively high S_v within the SSL (i.e., strong backscatter in the SSL
224 relative to the background level).

225 The upper and lower boundaries of the SSLs identified by the clustering algorithm were
226 imported to Echoview as editable line files to delineate SSL regions (e.g., red lines in Figure 2a
227 which delimit the upper and lower boundaries of the SSL associated with Cluster 0). The
228 broadband spectra of pulse-compressed volume backscattering strength ($S_v(f)$) was extracted
229 from each identified SSL using Echoview's "Wideband Frequency Response" export option.
230 Broadband frequency response values were converted to the linear domain (volume
231 backscattering coefficient spectra, $s_v(f)$). We selected a Fourier transform window size of 0.4
232 m at a frequency resolution of 100 Hz over the entire bandwidth for a total of 1001 values per
233 SSL. The Fourier transform window size was selected as a compromise between high frequency
234 resolution and a high range resolution (Benoit-Bird and Waluk, 2020). The median and the
235 interquartile range of $s_v(f)$ from each SSL were calculated for further analysis.

236 C. Sound scattering models

237 We ran scattering model ensembles per taxonomic group to calculate the theoretical
238 backscatter for the forward and inverse acoustic density estimates. The taxonomic groups
239 were selected from the net and trawl density data.

240 1. Weakly scattering fluid-like zooplankton

241 The weakly scatterers were copepods, euphausiid larvae, and amphipods, which were
242 modelled using a prolate spheroid for the copepods and a finite uniformly-bent cylinder for
243 the euphausiid larvae and amphipods. Weakly scatterers have a sound speed contrast (h) and
244 density contrast (g) of $1 \pm 5\%$. A near-unity sound speed and density contrast implies that the
245 material properties of the scatterers are not significantly different from the surrounding
246 medium (seawater). We chose the phase-compensated distorted wave Born approximation
247 (PC-DWBA) model for the weakly scatterers in our domain because it is specifically adapted
248 to densely aggregated zooplankton (Chu and Ye, 1999). Also, the PC-DWBA is adequate for
249 the range of fluid-like taxonomic groups in the Tromsøflaket epipelagic layer because the
250 parameters are flexible to geometry, material properties, and acoustic frequency changes
251 (Chu and Ye, 1999; Gastauer et al., 2019). We identified the most abundant species of each
252 taxonomic group to determine the model parameters. Copepods were modelled as *Calanus*
253 *finmarchicus copepodite stage V (CV)* (61% of copepods in the MultiNet samples,
254 Supplementary Materials Table S1), euphausiid larvae were modelled as *Thysanoessa*
255 *inermis* (100% of euphausiid larvae in the Tucker Trawl samples, Supplementary Materials
256 Table S2) and amphipods were modelled as *Themisto abyssorum* (100% of amphipods in the
257 MultiNet samples, Supplementary Materials Table S1). We ran 1000 model simulations for
258 each taxonomic group using the ZooScatR package (version 0.5; Gastauer et al., 2019) with

259 varying shape, size, and material properties parameters. These parameters were selected
 260 based on literature or net and trawl samples (Table 2). The length distribution for euphausiid
 261 larvae was calculated using the measurements of *Thyssanoessa inermis* in the Tucker trawl
 262 subsamples from stations 7, 8 and 9 (Figure 1). The length distribution for amphipods was
 263 identified by pooling measurements of *Themisto abyssorum* in MultiNet samples from
 264 stations 8-17 and Tucker Trawl samples from stations 7, 8 and 9. We repeated 1000 model
 265 simulations with random sampling within the distribution of each model parameter (Table 2)
 266 to calculate the variance in the cross-sectional backscatter across the available frequency
 267 spectrum (283-383 kHz) of each weakly scattering taxonomic group.

268 Table 2: PC-DWBA model parameter distributions for each taxonomic group. The distribution
 269 used are gamma: Γ (shape, rate), log normal: L (meanlog, sigmalog) and normal: N (mean,
 270 sigma).

Parameters	Copepods	Euphausiid larvae	Amphipods
Scattering model	DWBA Prolate spheroid	DWBA Uniformly-bent cylinder	DWBA Uniformly-bent cylinder
Length	$N(2.62, 0.09)^a$	$L(1.5, 0.3)^b$	$\Gamma(10.3, 2.3)^c$
Length-to-width ratio	$N(2.7, 0.2)^a$	$N(10.5, 0.3)^d$	$N(3, 0.5)^d$
Density contrast (g)	$N(0.996, 0.003)^{e,f}$	$N(1.036, 0.005)^e$	$N(1.058, 0.005)^d$
Sound speed contrast (h)	$N(1.027, 0.005)^e$	$N(1.026, 0.005)^e$	$N(1.058, 0.005)^d$
Orientation	$N(90, 30)^g$	$N(20, 20)^d$	$N(0, 30)^d$

271 ^aSantana Hernández (2019)

272 ^b Fit for the length measurements from the Tucker trawl subsamples. The distribution was assessed as
 273 the best fit based on a 1:1 line between theoretical and empirical quantile in Q-Q plots.

274 ^c Fit for the length measurements from MultiNet and Tucker trawl subsamples. The distribution was
 275 assessed as the best fit based on a 1:1 line between theoretical and empirical quantile in Q-Q plots.

276 ^dLavery et al. (2007)

277 ^eKögeler et al. (1987)

278 ^fChu and Wiebe (2005)

279 ^gBlanluet et al. (2019)

280 2. Elastic-shelled zooplankton

281 The pteropod taxonomic group was modelled (in Python version 3.7) with a viscous-elastic
282 model (Feuillade and Nero, 1998), as updated by Khodabandeloo et al. (2021). The model is
283 developed for shapes with four layers: gas layer (swimbladder), thin elastic layer
284 (swimbladder wall), thicker viscous layer (fish flesh) and the surrounding medium (seawater).
285 We adjusted the model for pteropods by reducing the thickness of the viscous layer to zero,
286 increasing the thickness of the elastic layer to correspond with the shell thickness, and
287 characterising the gas layer with the material properties of internal soft tissue. The
288 adjustments to the boundary conditions fitted with the literature description of pteropods, a
289 roughly spherical hard aragonite elastic shell with soft and weakly reflecting internal tissue
290 inside (Lavery et al., 2007; MacLennan and Simmonds, 2008). The model is parameterised by
291 the material properties and size of each layer, including the shape (thickness), density and
292 sound speed properties (Khodabandeloo et al., 2021). As with the weakly scatterers, we
293 identified the most abundant species to represent the taxonomic group in the scattering
294 model. The pteropods were modelled as *Limacina retroversa* (100% of pteropods in the
295 Tucker trawl samples, Supplementary Materials Table S2). We assumed a spherical target for
296 the scattering model. To account for the slightly elongated shape, we determined the radii
297 distributions using both the width and length of the subsampled *Limacina retroversa* from
298 the Tucker Trawl samples at stations 7, 8 and 9. The other shape parameters (radius of
299 viscous layer and radius of gas layer; parameterised as a dense fluid layer) were calculated for
300 each ensemble based on the selected elastic shell radius (Table 3). The outer layer was
301 parameterised as aragonite. The internal layer was parameterised as a dense fluid
302 representing the internal tissue with $g = 1.022$ and $h = 1.04$ (Lavery et al., 2007). The variance
303 from the parameter space of the viscous-elastic model was assessed by repeating 1000

304 model iterations with random sampling within the distribution of the radius of the elastic
 305 shell parameter (Table 3).
 306 Table 3: Viscous elastic model ensemble shape and material properties parameters for
 307 pteropods and fish larvae in Tromsøflaket.

Shape (mm)	Pteropods (<i>two-layer sphere</i>)	Fish larvae (<i>three-layer sphere</i>)
Radius of elastic shell - R_3	$\Gamma(\text{shape}= 5.4, \text{rate}= 9.17)^a$	$\text{Lognormal}(-1.46, 0.45)^b$
Radius of viscous layer - R_2	R_3	$(8.77 * R_3) + 1.62^c$
Radius of gas layer - R_4	$R_3 - (0.023 * R_3)^d$	$R_3 - 0.01^e$
Density (kg/m³)		
Surrounding medium - ρ_1	1027 ^d	1027 ^d
Viscous layer - ρ_2	n/a	1040 ^e
Elastic layer - ρ_3	2920 ^f	1141 ^g
Gas layer - ρ_4	1050 ^h	325.1 ^e
Sound speed (m/s)		
Surrounding medium - c_1	1480 ⁱ	1480 ⁱ
Viscous layer - c_2	n/a	1522.92 ^e
Elastic layer - c_3	5219 ^{e,j}	1450 ^e
Gas layer - c_4	1522.92 ^{h,j}	325.1 ^e
Shear viscosity (N/m²) - μ_2		
Shear viscosity (N/m ²) - μ_2	n/a	0.8571 ^{e,g}
Shear modulus (MPa) of swimbladder wall - μ_3		
Shear modulus (MPa) of swimbladder wall - μ_3	35800 ^j	0.17 ^e

308 ^a Fit for the length measurements and corresponding widths using length-to-width ratio from Stanton
 309 et al. (2000) ($L/a = 1.5$). The distribution was assessed as the best fit based on a 1:1 line between
 310 theoretical and empirical quantile in Q-Q plots.

311 ^b Swimbladder radius was calculated based on the measured total length and the calculated widths
 312 using the relationship described by the data in Chu et al. (2003) and assuming a linear relationship (R^2
 313 = 0.98), as shown in Figure S1. The distribution was assessed as the best fit based on a 1:1 line
 314 between theoretical and empirical quantile in Q-Q plots.

315 ^c Linear regression (Supplementary material; Figure S1) established from swimbladder length-to-total
 316 length relationship using data from Chu et al. (2003).

317 ^d Subtracted shell layer thickness (2.3% of radius) from elastic shell radius based on value from Lavery
 318 et al. (2007)

319 ^e Khodabandeloo et al. (2021)

320 ^f Stanton et al. (2000)

321 ^g Feuillade and Nero (1998)

322 ^hLavery et al. (2007)

323 ⁱShip-based CTD measurements

324 ^jLiu et al. (2005)

325 3. Gas-bearing organisms

326 The fish larvae taxonomic group was modelled with the viscous-elastic model as
327 juvenile/larvae of *Gadus morhua* (70% of fish larvae in the Tucker Trawl, Supplementary
328 Materials Table S2). The main scattering component of a gas-bearing organism is the gas
329 enclosure, in this case the swimbladder. The radius of the elastic shell, the swimbladder
330 including the swimbladder wall, was calculated by converting total length measurements to
331 swimbladder length using relationships from juvenile and larval *Gadus morhua* studied by
332 Chu et al., 2003 (Supplementary Materials Figure S1). The corresponding swimbladder widths
333 were also calculated through a swimbladder length-to-volume linear relationship, assuming a
334 prolate spheroid swimbladder shape (Chu et al., 2003). The viscous-elastic model comparison
335 of a sphere and a prolate spheroid at a range of incident angles indicates that the magnitude
336 of the frequency response is dependent on the local radius at the angle of incidence (Figure
337 10 in Khodabandloo et al., 2021). The peaks and nulls are horizontally translated, but these
338 are eliminated through averaging for the volume backscatter of an aggregation. Therefore,
339 we assumed a spherical target and determined the distribution of radii of the fish larvae
340 using swimbladder length and width (R3 in Table 3). The radii distributions were determined
341 from the measured juvenile/larvae *Gadus morhua* from the Tucker Trawl samples at stations
342 7, 8 and 9.

343 The other shape parameters (radius of the viscous layer and the gas layer) were calculated
344 for each model simulation iteration based on the randomly selected elastic shell radius (Table
345 3). The variance from the parameter space of the viscous elastic model was assessed by

346 repeating 1000 model iterations with a random selection of parameters given the
347 distributions in Table 3.

348 D. Density estimates

349 The acoustic density estimates are based on the linearity principle that the total scattered
350 energy from a volume is equal to the sum of the scattered energy of each randomly
351 distributed individual scatterers within that volume (Foote, 1983; Greenlaw, 1979; Lavery et
352 al., 2007), given by:

$$353 \quad s_v(f) = \sum_{i=1}^N \sigma_{bs}^i(f) * \rho^i$$

354 *(Equation 2)*

355 Where $s_v(f)$ is the volume backscattering coefficient spectra in m^2 per m^3 with
356 measurements at all frequencies f in Hz, N is the number of taxonomic groups in the sampled
357 volume, $\sigma_{bs}^i(f)$ is the cross-sectional backscatter spectra of a given taxonomic group i at all
358 frequencies f in m^2 , and ρ^i is the density in individuals per m^3 (ind. m^{-3}) for each taxonomic
359 group i .

360 Estimates based on this equation assume that the entire volume backscatter is formed by the
361 species or taxonomic groups included in the cross-sectional backscatter term. For the
362 forward and inverse methods, we assumed the intensity of the backscattered signal was
363 solely from the five modelled taxonomic groups.

364 1. Forward method

365 The forward method is an approach to calculate density or biomass estimates of taxonomic
366 groups from hydroacoustic-trawl survey data (Love, 1975; Davison et al., 2015; Dornan et al.,

367 2022). The forward method for density estimates, as described in MacLennan and Simmonds,
368 2008, was computed at the nominal frequency (333 kHz) to emulate the results from a
369 narrowband (single frequency) survey, which simplifies Equation 2 to:

$$370 \quad s_v = \langle \sigma_{bs} \rangle * \rho^{total}$$

371 *(Equation 3)*

372 where s_v is the volume backscattering coefficient at a given frequency, $\langle \sigma_{bs} \rangle$ is the average
373 predicted cross-sectional backscatter weighted by the relative density from net and trawl
374 sampling, and ρ^{total} is the total density in individuals per m^3 (ind. m^{-3}).

375 We extracted the median s_v at the nominal frequency from the median $s_v(f)$ of each SSL.
376 From the scattering model simulations for each taxonomic group, we extracted the weighted
377 average $\langle \sigma_{bs} \rangle$ at the nominal frequency. The weights were calculated by the mean of the
378 relative densities from the MultiNet and Tucker trawl samples (Supplementary Materials
379 Table S3 and Table S4). The calculated ρ^{total} for each SSL was divided among the taxonomic
380 groups based on the relative density.

381 2. Inverse method

382 Alternatively, the inversion of the broadband scattering data can be used to solve Eq. 1 with a
383 least-squares data fitting solver, as in Lavery et al., 2010 (Greenlaw, 1979; Lavery et al.,
384 2007). From the scattering model simulations for each taxonomic group, we calculated the
385 median cross-sectional backscatter, $\sigma_{bs}^i(f)$ (Eq. 2) and 90% bootstrap interval of the median
386 across the frequency spectrum. To calculate the density of each taxonomic group for the
387 autonomous hydroacoustic survey with the inverse method, we solved Equation 2 for density
388 ρ^i as a linear least-squares problem by using a Trust Region Reflective algorithm as described
389 in Branch et al. (1999). The optimiser (Python version 3.7, `scipy.optimize.lsqr_linear`)

390 determined the best solution by minimising the following problem with the following bounds

391 ($0 \leq \rho^i < \infty$):

$$392 \quad 0.5 * \left| \left| \sigma_{bs}^i(f) * \rho^i - s_v(f), \right| \right|^2$$

393 (Equation 4)

394 A sensitivity analysis was conducted to quantify the effect of altering species shape and
395 material properties on the variability of the inverse method density estimates. We ran 500
396 random permutations of Eq. 3 with replacement. The cross-sectional backscatter spectra of
397 each species varied between the median, the 5th and 95th percentiles. The $s_v(f)$ of each SSL
398 varied between the median and the interquartile range.

399 IV. Comparison analysis

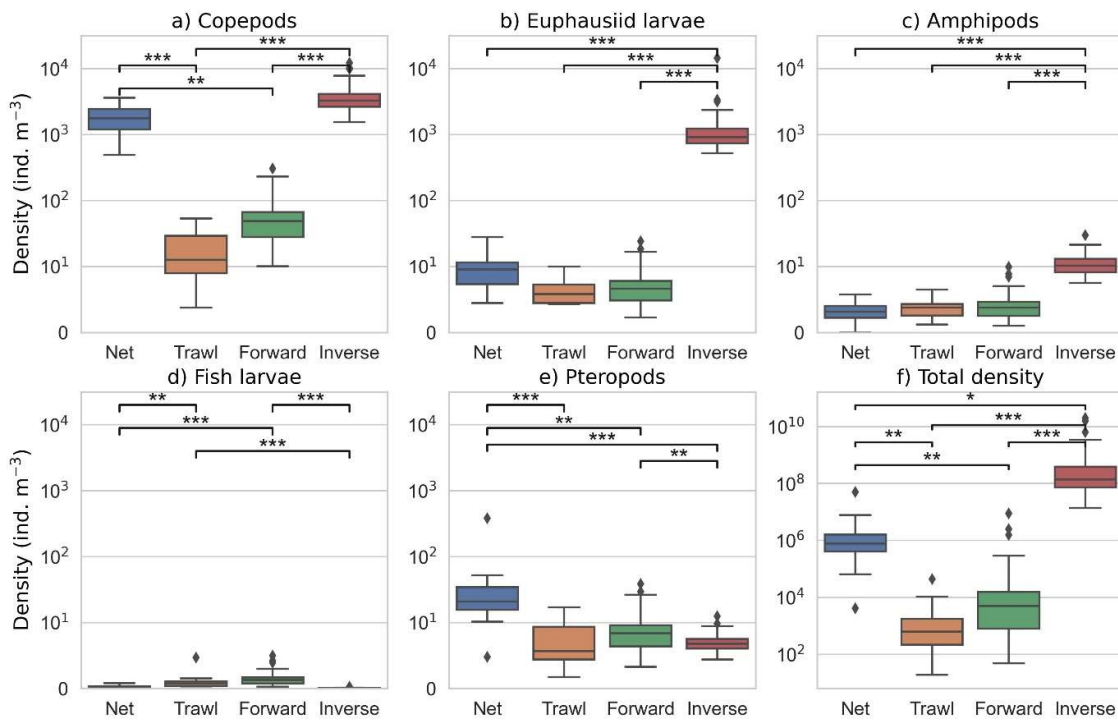
400 For comparison across all four methods, we performed a Kruskal-Wallis H test. For non-
401 parametric pairwise comparisons, Dunn's tests were computed with p-values adjusted with
402 the Benjamini-Hochberg adjustment (non-negative) to assess the significance of the
403 difference in density estimates between each method pair for each taxonomic group.

404 Results

405 I. Biological sampling

406 Copepods dominated the mesozooplankton community sampled with the MultiNet with a
407 mean density with standard error (\pm SE) of 1800 ± 300 ind. m^{-3} (95% of the density, Figure 3).
408 Pteropods were the second most abundant taxonomic group in the MultiNet samples, with a
409 mean density of 50 ± 30 ind. m^{-3} . Euphausiid larvae had a low density (9 ± 2 ind. m^{-3} , 0.5% of
410 the community); most of these were represented by euphausiid larvae in *furcilia* stages (89%

411 of euphausiid larvae over all MultiNet samples). Other species, such as siphonophores and
 412 meroplankton, not included in the selected taxonomic group for this study, accounted for 30
 413 ± 5 ind. m^{-3} , or 2%, of the MultiNet catch in the study region. Detailed MultiNet density data
 414 are presented in Supplementary Materials Table S1 and Table S3.



415
 416 Figure 3: a-e) Density estimates in the logarithmic domain for each dominant taxonomic
 417 group in Tromsøflaket, in units of base 10 logarithm of individuals per m^3 . Each box
 418 summarises the density measurement from Net (MultiNet; n=11, blue), Trawl (Tucker trawl;
 419 n=11, orange), Forward (acoustic forward method; n=70, green) or Inverse (acoustic inverse
 420 method; n=70, red). Significant differences are denoted by the number of asterisks (*), with
 421 *** $p < 0.001$, ** $p < 0.01$ and * $p < 0.05$ from pairwise Dunn's tests. f) is the total density
 422 estimate (sum of all species) for all stations (Net and Trawl) and all SSLs (sound scattering
 423 layers) (Forward and Inverse). Note the different y-axis scale in subplot f.

424 Like the MultiNet samples, the Tucker trawl samples were primarily composed of copepods
 425 (54% of the community, Figure 4), but the average density was much lower with 19 ± 5 ind.
 426 m^{-3} (Figure 3). Small pteropods (mean length = 1.2 mm, Table 4) were the second most
 427 abundant taxonomic group in the trawl samples, with a mean density of 5 ± 1 ind. m^{-3} (17%
 428 of the community). Euphausiid larvae had comparable density (3.5 ± 0.7 ind. m^{-3} , 16% of the
 429 community); most of these larvae were *Thyssanoessa inermis* (99.8% of euphausiid larvae in
 430 the Tucker Trawl sample). The mean length of the larvae was 4.7 mm suggesting they were
 431 still young of the year, like the furcilia stages from the MultiNet samples (mean length 4.0
 432 mm; Table 4). Other species not included in the selected taxonomic group for this study, such
 433 as siphonophores and decapod crustaceans, accounted for 7% of the Tucker trawl catch in
 434 the study region. Detailed Tucker trawl density data are available in Supplementary Materials
 435 Table S2 and Table S4.

436 Table 4: The size distribution of the dominant species from each taxonomic group. MultiNet
 437 and Tucker trawl length measurements were taken from subsamples. The "acoustics"
 438 sampling method shows the mean length and standard deviation used in the scattering
 439 models for the forward and inverse methods.

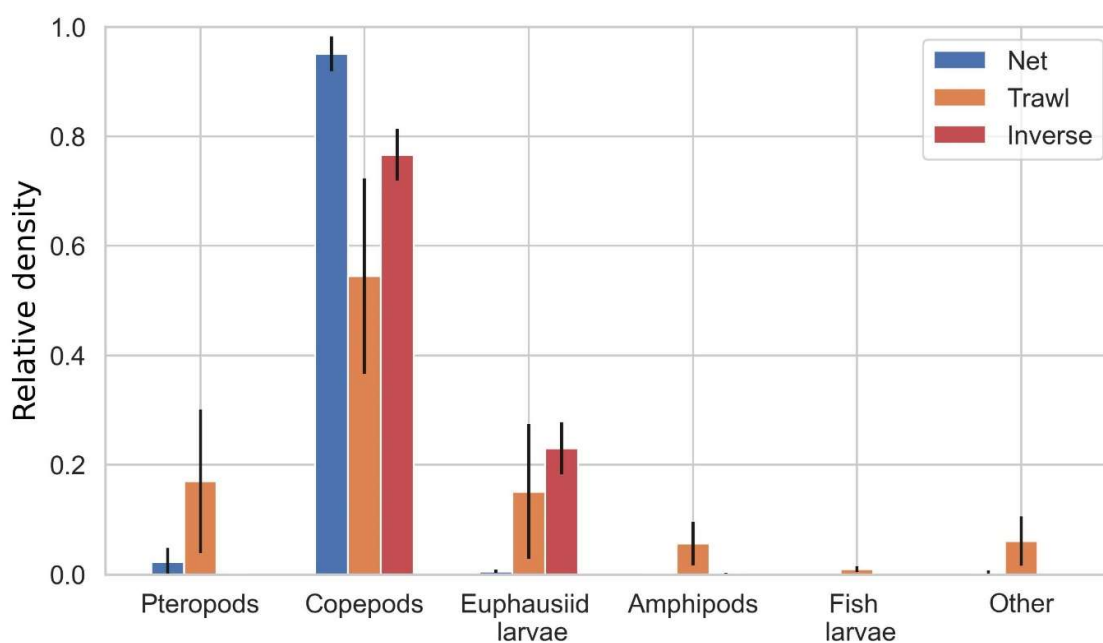
Taxonomic group	Sampling method	Species	N	Mean length (mm)	Sd of length (mm)
Pteropods	MultiNet	<i>Limacina retroversa</i>	157	1.5	0.6
	Tucker trawl	<i>Limacina retroversa</i>	70	1.2	0.3
	Acoustics	<i>Limacina retroversa</i>	229	1.4	0.6
Copepods	MultiNet	<i>Calanus finmarchicus CV</i>	^a	2.62 ^b	0.09
	Tucker trawl	<i>Calanus finmarchicus CV</i>	n/a	n/a	n/a
	Acoustics	<i>Calanus finmarchicus CV</i>	^a	2.62 ^b	0.09
Euphausiid larvae	MultiNet	Euphausiacea furcilia	105	4.0	1.0
	Tucker trawl	<i>Thyssanoessa inermis</i>	108	4.7	1.6
	acoustics	<i>Thyssanoessa inermis</i>	108	4.7	1.6

Amphipods	MultiNet	<i>Themisto abyssorum</i>	75	4.6	1.4
	Tucker trawl	<i>Themisto abyssorum</i>	108	4.3	1.2
	Acoustics	<i>Themisto abyssorum</i>	183	4.4	1.3
Fish larvae	MultiNet	<i>Pisces larvae</i>	8	8.3	5.8
	Tucker trawl	juvenile/larvae <i>Gadus morhua</i>	61	9.3	3.2
	Acoustics	juvenile/larvae <i>Gadus morhua</i>	61	7.6	3.1

440 Note: All measurements are of full length unless otherwise specified.

441 ^aSantana Hernández (2019)

442 ^bProsome Length (PL)



443

444 Figure 4: Relative density of each taxonomic group as calculated by each sampling method

445 across the whole survey region of Tromsøflaket with standard deviation error bars

446 representing variability between stations (Net and Trawl) or SSLs (Inverse). Taxonomic groups

447 are ordered from smallest (left) to largest (right). Size details of each taxonomic group are

448 described in Table 4.

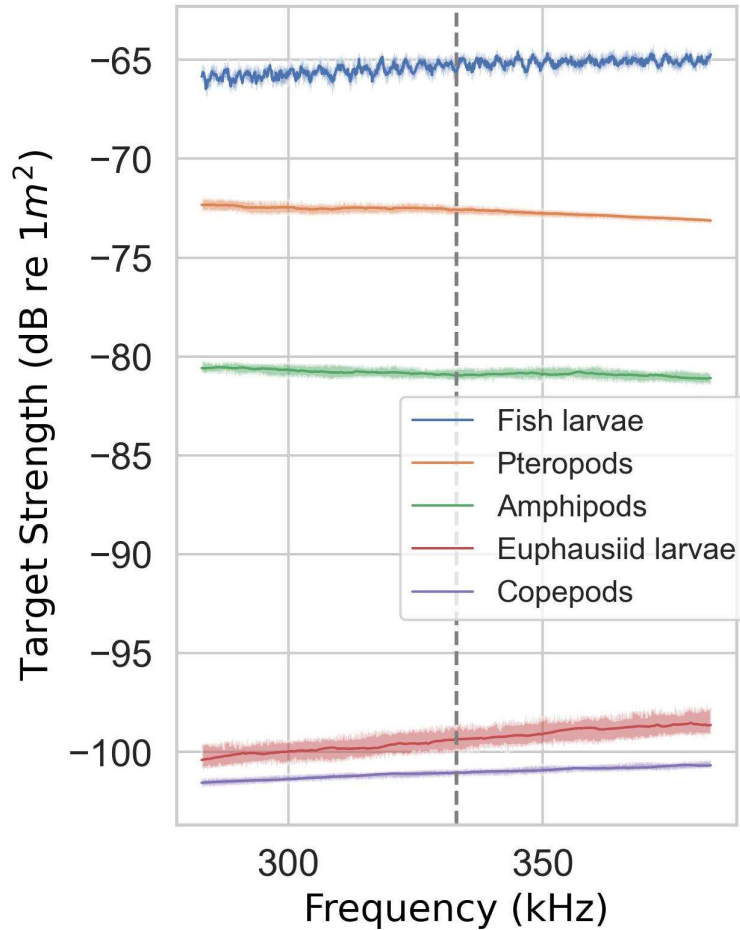
449 II. Acoustics

450 A. Sound scattering layer detection

451 The k-means clustering algorithm identified a total of 70 SSLs over the autonomous acoustic
452 survey period. The SSLs varied between 1 m to 29 m (min. and max.) in thickness, with the
453 layers centred at an average depth of 20.6 m. The median volume backscattering strength
454 spectra from all the SSLs varied between -75 to -50 dB re 1 m⁻¹ (min. and max.). At the
455 nominal frequency, the median $S_v(f)$ varied between -73 and -56 dB re 1 m⁻¹ (min. and max.).

456 B. Scattering models

457 The target strength (TS) frequency response varied in strength and shape across the
458 taxonomic groups. The median broadband TS ranged from a minimum of -100 dB re 1 m² at
459 the lowest frequency, 283 kHz, for the smallest fluid-like weakly scatterer, copepod
460 taxonomic group, to a maximum of -65 dB re 1 m² at 345 kHz from the gas-bearing
461 taxonomic group, fish larvae (Figure 5). Copepods, euphausiid larvae and fish larvae TS
462 spectra had a positive slope with TS increasing with frequency, whereas amphipods and
463 pteropods had a negative sloping TS(f) (Supplementary Materials Figure S2, shown as cross-
464 sectional backscatter spectra, i.e., linear form of TS). The cross-sectional backscatter matrix
465 had a rank of 5, suggesting the taxonomic groups were linearly independent and can be
466 distinguished by the least-squares algorithm.



467

468 Figure 5: Median target strength results of ensemble simulations from the scattering models
 469 for each dominant taxonomic group in Tromsøflaket, including the 90% bootstrap confidence
 470 intervals of the median as the shaded region. Vertical grey gashed line indicates the nominal
 471 frequency (333 kHz).

472 C. Forward method density estimates

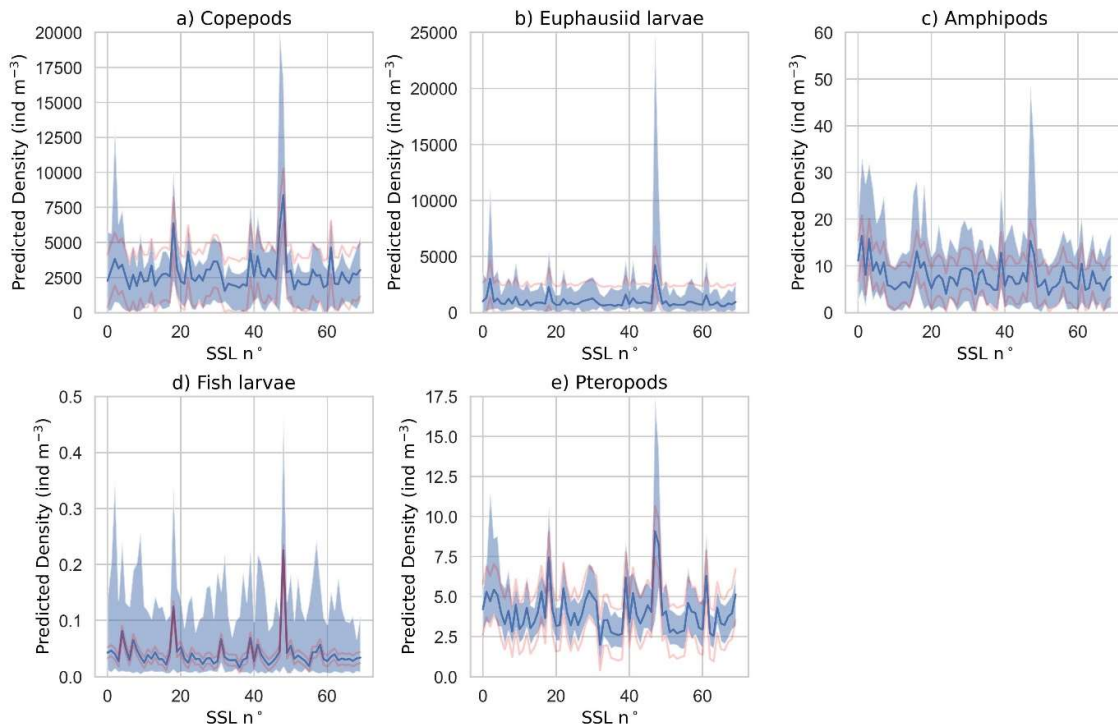
473 Based on the relative density results from the MultiNet and Tucker trawl, the forward
 474 method estimated SSLs dominated by copepods ($56 \pm 6 \text{ ind. m}^{-3}$) followed by pteropods (7.0
 475 $\pm 0.7 \text{ ind. m}^{-3}$), euphausiid larvae ($4.3 \pm 0.5 \text{ ind. m}^{-3}$), amphipods ($1.6 \pm 0.2 \text{ ind. m}^{-3}$) and fish

476 larvae (0.40 ± 0.04 ind. m^{-3}) (Figure 3). The relative density was a fixed input parameter in the
477 calculation; therefore, the forward method was not included in Figure 4.

478 D. Inverse method density estimates

479 The density estimates measured from the inversion of the autonomous acoustic survey
480 showed an SSL dominated by the copepods (3700 ± 200 ind. m^{-3} ; 77% of acoustic density
481 estimates), which agreed with the MultiNet results. The second most abundant group in the
482 acoustic results was euphausiid larvae (modelled as *Thyssanoessa inermis* from Tucker trawl),
483 with 1300 ± 200 ind. m^{-3} , representing 23% of the total taxonomic composition. In the
484 inverse method estimates, amphipods had a higher density than pteropods with 10.3 ± 0.5
485 ind. m^{-3} (0.2%) and 3.9 ± 0.2 ind. m^{-3} (0.08%), respectively. The fish larvae had the lowest
486 density as with the other sampling methods, 0.126 ± 0.001 ind. m^{-3} ; 0.002% of the total
487 composition.

488 The sensitivity analysis showed the variability in the density estimates compared to the
489 variation in the model parameters and the volume backscatter within each SSL (standard
490 deviation). The sensitivity of density estimates was compared to the distribution of densities
491 of the 70 SSLs. For the copepods and euphausiid larvae, the effect of the dispersion in the
492 model parameters and volume backscatter variability was smaller than the standard
493 deviation from the density estimates of all the SSLs (Figure 6 a, b). Conversely, amphipods,
494 fish larvae and pteropods density estimates had a larger sensitivity to the model parameters
495 and volume backscatter than the variability in density estimates across the study region
496 (Figure 6 c, d, e). Density estimates of all species showed higher variability in the case of SSLs
497 with high backscatter (e.g., SSL n° 47-48; Figure 6).



498

499 Figure 6: The sensitivity analysis results for predicted density estimates of each taxonomic
 500 group (a-e) for the inversion of acoustic data with scattering model results varying randomly
 501 between median, the 5th and 95th percentiles and the volume backscatter spectra varying
 502 randomly between median, and interquartile range for each SSL (x-axis). The blue line in each
 503 panel is the median of the sensitivity analysis, the shaded region displays the extent of the 5th
 504 and 95th percentile. The red lines indicate the standard deviation of the density estimates for
 505 all the SSLs. Note the difference in scale of the y-axis.

506 III. Density analysis across methods

507 All four methods compared in this analysis (MultiNet, Tucker trawl, and forward and inverse
 508 method with autonomous acoustic survey data) showed that copepods dominated the
 509 epipelagic SSL across the study area (> 50% density for all sampling methods, Figure 4).
 510 However, comparisons of density estimates for all methods were significantly different for

511 each taxonomic group as revealed by a Kruskal-Wallis H test, denoted with degrees of
512 freedom in parenthesis (copepods: $H(3) = 127.87$, $p < 0.0001$; euphausiid larvae: $H(3) =$
513 121.24 , $p < 0.0001$; amphipods: $H(3) = 115.14$, $p < 0.0001$; fish larvae: $H(3) = 118.10$, $p < 0.0001$;
514 pteropods: $H(3) = 31.89$, $p < 0.0001$) (Figure 3).

515 Density estimates were significantly different between the MultiNet and Tucker trawl for
516 copepods, pteropods, and fish larvae (Dunn's test; $p < 0.01$). No significant differences in
517 density estimates between the net and trawl were found for the other taxonomic groups
518 (euphausiid larvae: $p = 0.19$ and amphipods: $p = 0.79$). Results from pairwise comparisons from
519 Dunn's tests are shown in Figure S3 (in Supplementary Materials). Density estimates of
520 euphausiid larvae were almost three times higher based on the MultiNet samples than the
521 Tucker trawl samples. However, the relative density of euphausiid larvae in the Tucker trawl
522 samples was higher (11.1%) than in the MultiNet samples (0.5%) (Figure 4). As with the
523 euphausiids, pteropods density was eleven times higher in the MultiNet samples than in the
524 Tucker trawl samples, but pteropods had a lower relative density in the MultiNet (2.8% of the
525 community) than in the Tucker Trawl (16.1%). For amphipods, similar densities were sampled
526 by net and trawl (1.2 ± 0.3 ind. m^{-3} for MultiNet and 1.4 ± 0.3 ind. m^{-3} for Tucker trawl). Fish
527 larvae were found in low densities, on average 0.05 ± 0.02 ind. m^{-3} in the MultiNet and $0.3 \pm$
528 0.2 ind. m^{-3} in the Tucker trawl, and had low relative densities in both net and trawl ($< 1\%$ of
529 the total catch in both direct sampling methods).

530 A pairwise comparison of the forward method for acoustic data analysis showed that these
531 density estimates were not statistically different from the Tucker trawl estimates for all
532 taxonomic groups (copepods: $p = 0.08$; euphausiid larvae: $p = 0.77$; amphipods: $p = 0.79$; fish
533 larvae: $p = 0.31$; pteropods: $p = 0.07$). In contrast, density estimates from the forward method

534 were statistically different from estimates from the MultiNet samples for copepods ($p < 0.01$),
535 fish larvae ($p < 0.001$) and pteropods ($p < 0.01$), but not for the euphausiid larvae ($p = 0.18$) and
536 amphipods ($p = 0.76$). The density estimates calculated from the autonomous acoustic survey
537 data by the forward and inverse methods were statistically different for all taxonomic groups
538 ($p < 0.01$).

539 Pairwise comparisons indicated that the autonomous acoustic survey density estimates
540 calculated through inversion differed significantly from the other sampling methods for the
541 euphausiid larvae and amphipods (Dunn's test; $p < 0.001$). However, for the copepods, the
542 inverse results were not statistically different from the MultiNet ($p = 0.06$) but statistically
543 different from Tucker trawl ($p < 0.001$). The results from the inverse method were not
544 statistically different from densities measured from the Tucker trawl for pteropods ($p = 0.92$)
545 but were statistically different from the results of the MultiNet and forward method ($p < 0.01$).
546 For fish larvae, the densities measured from the MultiNet were not statistically different from
547 the results of the inverse method ($p = 0.58$) but were statistically different from the densities
548 measured from the Tucker trawl and forward method ($p < 0.001$).

549 Overall, the inverse method reported the highest total average density of 4987 ind. m^{-3} ,
550 followed by the MultiNet samples (1931 ind. m^{-3}), the forward method (70 ind. m^{-3}) and the
551 Tucker trawl samples (29 ind. m^{-3}).

552 Discussion

553 I. Comparison of sampling methods

554 To our knowledge, this study is one of the first implementations of the inverse method from
555 an autonomous broadband acoustic survey with TS estimates informed by locally derived

556 measurements of shape properties. The inverse method yielded higher density estimates.
557 These density estimates are most likely a more accurate representation of the sound
558 scattering layers for the five dominant plankton taxonomic groups in the Norwegian Sea. Net
559 and trawl sampling likely underestimated zooplankton densities within the SSL because of
560 gear-specific biases when assessing species composition across size classes (Skjoldal et al.,
561 2013; Hetherington et al., 2022).

562 All sampling methods determined that copepods dominated the epipelagic SSL in
563 Tromsøflaket. The relative density of copepods calculated from the inverse method (77%)
564 was between the MultiNet (95%) and Tucker trawl (54%). We suspect that because the
565 copepods were relatively large individuals (mainly *Calanus finmarchicus* CV with a mean
566 length of 2.6 mm) organised in dense swarms, the high frequency and high bandwidth (283-
567 383 kHz) of the acoustic instrument detected most of these copepods. The agreement of the
568 density estimates from the inverse method and MultiNet suggests that the high vertical
569 resolution of the broadband acoustic data could be used to increase the accuracy of copepod
570 density estimates within the epipelagic layer. In the future, satellite observations of ocean
571 colour could compensate for the blind zone of acoustic measurements near the surface and
572 measure the near-surface density of copepods (Basedow et al., 2019).

573 Variations in organism size and swimming abilities must be considered when designing
574 surveys and selecting sampling methods. The MultiNet targets small zooplankton species
575 (>0.3 mm), especially weak swimmers aggregating in high densities. The Tucker trawl is
576 designed to catch larger, fast-swimming zooplankton and ichthyoplankton species in the
577 epipelagic layer. Therefore, we did not expect to find higher densities of euphausiid larvae in
578 the MultiNet compared to the Tucker trawl since they are known to avoid MultiNets and

579 similar gear (Brinton, 1967; Greenlaw, 1979). The inverse method estimated densities of
580 euphausiid larvae as more than 100 times higher than the net, trawl, and forward method.
581 Because of the well-known ability of euphausiids to avoid capture by standard oceanographic
582 nets (Wiebe et al., 1982), we suggest that the density estimates of euphausiid larvae based
583 on the inverse method are likely closer to reality than the estimates based on the compared
584 methods. Both the MultiNet and Tucker trawl captured small euphausiids (mean length in
585 MultiNet = 4.0 mm and mean length in Tucker trawl = 4.7 mm, Table 4), which did not have
586 the backscattering properties of adults. Young euphausiids have less than 30% of the lipid
587 content of adults, which reduces their density contrast (Kögeler et al., 1987). We expect the
588 density difference of the net, trawl, and forward method to the inverse method to be even
589 larger in the case of adult euphausiids because of their increased avoidance abilities and
590 stronger sound scattering properties.

591 The relatively high densities of both small (copepods) and larger mobile (amphipods and
592 euphausiids) zooplankton measured with the inverse method suggests that this approach can
593 accurately sample a larger size spectrum of targets than the other methods. Similar to
594 euphausiids, density estimates of amphipods were higher when calculated with the inverse
595 method. Amphipods are also fairly strong scatterers and mobile swimmers (Skjoldal et al.,
596 2013). We conclude that the inverse method from autonomous acoustic surveys provided
597 the best density estimates for agile organisms that avoid nets and trawls.

598 The inverse acoustic method could be applied to larger organisms than zooplankton, such as
599 pelagic fish. Sampling efficiency for fish and their vertical distribution in the water column has
600 been widely studied because of the socio-economic importance of fisheries (Handegard and
601 Tjøstheim, 2005). A net comparison study from June 1993 in Storfjorden, Norway, has

602 reported a higher density of ichthyoplankton between 50-100 m than between 0 – 50 m
603 (Skjoldal et al., 2013). The autonomous acoustic monitoring system used in this study had a
604 maximum depth of 50.5 m, limiting the detection of fish larvae in deeper regions of the
605 epipelagic layer. Yet, ichthyoplankton densities were comparable between methods. One way
606 of improving estimates of density and vertical distribution pattern of fish larvae in high
607 latitude shelf areas could be to use the inverse method with a transducer with a deeper
608 detection range (lower frequency band or longer pulse length) or using both surface and
609 underwater vehicles, such as gliders. A lower frequency bandwidth (for example, 185-255
610 kHz) would also be beneficial for measuring the density of ichthyoplankton and pteropods
611 because they have a stronger acoustic backscatter at lower frequencies.

612 Zooplankton layers are known to exhibit patchiness; therefore, variability in relative density
613 across the sampling region is expected (Trevorrow et al., 2005, Basedow et al., 2006,
614 Trudnowska et al., 2016). For example, we found high variability in pteropod densities based
615 on net samples between stations (maximum at station 13 with 379 ind. m^{-3} and minimum at
616 station 17 with 2 ind. m^{-3}), which likely results from their patchy distribution (Elizondo and
617 Vogt, 2022). The Tucker trawl did not capture such a broad variability in densities (maximum
618 at station 8 with 16 ind. m^{-3} and a minimum at station 17 with 0.5 ind. m^{-3}), which may be
619 due to the larger mesh underestimating the small pteropods (mean length of 1.2 mm; Table
620 4). Because the net and trawl sampling and the acoustic measurements are not coincident in
621 time and space in this study, we used a static average relative density to reflect the species
622 composition of the region. In contrast, the inverse method provides continuous
623 measurements and is not dependant on punctual sampling.

624 II. Assessment of the autonomous acoustic survey and inverse 625 method for density estimates

626 Autonomous acoustic surveys require effective data processing methods that limit the
627 introduction of biases and can quickly be applied to large datasets. The results of the k-means
628 clustering algorithm revealed that, despite being ubiquitous over the study area, the sound
629 scattering layer varied in thickness, volume backscattering strength, and depth over time and
630 space. This algorithm restricted the user bias of identifying boundaries and increased
631 reproducibility because the only subjective parameter in this machine learning algorithm was
632 the number of clusters. The successful application of the k-means clustering method for
633 identifying SSLs in the Tromsøflaket area suggests that it can now be tested on more complex
634 vertical structures with multiple discrete SSLs in different regions.

635 Density estimates were corrected for the sampling volume for each method; however, the
636 differences in sampling depths could influence the results. The acoustic estimates were
637 bounded by the edges of the epipelagic SSLs which were determined by k-mean clustering
638 and typically found between 3.5 – 50 m, whereas the Tucker trawl sampled 0 – 20 or 40 m
639 and the MultiNet sampled 0 – 100 m. The acoustic density estimates did not incorporate
640 volumes with lower densities above and below the epipelagic SSL. In contrast, the densities
641 calculated from nets and trawls were averaged over the entire sampling range. The acoustic
642 inversion was only applicable within the boundaries of the SSL where the density of
643 scatterers is high. If the density of scatterers is too low, the echo statistics are dependent on
644 the target's location in the beam rather than the intensity summation process (Holliday and
645 Pieper, 1995). Under such low-density scenarios, single echo detections and echo counting
646 (Keiser and Mulligan, 1984; Simmonds and MacLennan, 2008) should be used instead of the

647 inverse method. However, if differences in density estimates were driven by differences in
648 sampling depths, we would expect high densities from both acoustic methods, not just the
649 inverse method.

650 In this study, we relied on the size distribution of the dominant species locally derived from
651 nets and trawls to inform the scattering models because the 283-383 kHz bandwidth only
652 detected the geometric scattering of the targets ($ka > 1$; Lavery et al., 2010). However, with a
653 broader frequency spectrum that captures the Rayleigh-to-geometric scattering transition of
654 all taxa, the size classes can be identified within the inverse method (Greenlaw, 1979; Lavery
655 et al., 2007; Cotter et al., 2021). In that case, the scattering transition point determines the
656 resonance frequency, which is inversely proportional to the size of the scatterers and can
657 increase the ability to differentiate among taxa (Holliday and Pieper, 1995; Warren et al.,
658 2003; Benoit-Bird, 2009). Capturing the Rayleigh-to-geometric transition would thus improve
659 the method because it produces a frequency response curve with a more identifiable shape
660 (Cotter et al., 2021). Nonetheless, we demonstrated that relying on a bandwidth covering the
661 transition point is not necessary to determine the density of epipelagic organisms using the
662 inverse method when size distributions are provided by net and trawl samples.

663 The sensitivity analysis tested the variability in the frequency-response curves compared to
664 the variability in the model parameters and showed that the density estimates of the
665 stronger scatterers (amphipods, fish larvae and pteropods) had a larger sensitivity to the
666 model parameters than the weaker scatterers (copepods and euphausiid larvae). The inverse
667 method is based on absolute scattering levels, which rely heavily on calibration (Lavery et al.,
668 2007). A two-sphere calibration covering the entire broadband signal should be carefully
669 completed for future density calculations using the inverse method. Careful calibration across

670 the bandwidth is critical, as with multi-frequency analysis, to avoid artificial trends in the
671 frequency-response curves. In addition, the inverse method requires knowledge of the
672 scattering model parameters for each taxonomic group. Here, some of these parameters
673 were informed by the net and trawl data but others were defined based on previous
674 literature values. Variability in model parameters like orientation or material properties can
675 affect the density estimates, especially for the stronger scatterers as shown by the sensitivity
676 analysis. *In situ* measurements of material properties, sound speed, and density contrasts,
677 and more knowledge about the orientation of the scatterers would restrict the variability of
678 model simulation results and improve the accuracy of the density estimates.

679 Because of their low taxonomic resolution, both the forward and inverse acoustic methods
680 are dependent on the initial taxonomic group selection. Different statistical or data-fitting
681 approaches with an error term could better account for non-dominant species, such as
682 meroplankton and decapod larvae. In the current study, errors in the taxonomic classification
683 would lead to a positive bias in the density estimates from the acoustic methods. The limited
684 taxonomic resolution of the acoustic inversion method could be improved by the addition of
685 imaging sensors which are already being integrated on autonomous platforms equipped with
686 a wideband echosounder (Whitmore et al., 2019; Reiss et al., 2021). Optical sensors could
687 also provide information on the size and, to some extent, the orientation of the scatterers
688 (Ohman et al., 2019), which would improve the *in situ* scattering models.

689 Conclusion

690 The inverse method was used to quantify aggregations of zooplankton and ichthyoplankton
691 with a broadband autonomous hydroacoustic survey and detected higher densities of
692 abundant mobile zooplankton than the net, trawl, and forward acoustic method. The inverse

693 method also detected similar densities of smaller mesozooplankton to the net samples. We
694 conclude that it is the most accurate method to measure the density of a broad size
695 spectrum of zooplankton, and most likely of ichthyoplankton and pelagic fish. This work built
696 on studies on the inverse method for zooplankton layers (Lavery et al., 2007), autonomous
697 hydroacoustic surveys (De Robertis et al., 2019) and broadband data processing (Basset et al.,
698 2019, Benoit-Bird and Waluk et al., 2020) in recent years. We further advanced the field by
699 offering a solution for the limitation of sparse coexisting biological sampling from
700 autonomous acoustic surveys by using the inverse method with locally derived size
701 measurements.

702 Accurate density estimates of pelagic organisms with high spatio-temporal resolution are
703 critical to conducting stock assessment surveys and understanding the impact of changes in
704 the epipelagic zone and their effects on food supply to deeper water ecosystems (Rogers,
705 2015). To this end, we conclude that applying the inverse method to broadband
706 hydroacoustic data can improve the accuracy of acoustic-trawl surveys. We further envision
707 that applying the inverse method to acoustic data collected from autonomous platforms
708 could supplement and extend the spatial resolution of vessel-based surveys at a lower cost
709 than additional ship time.

710

711

712

713

714

715 **Acknowledgement**

716 The authors thank Babak Khodabandeloo and Sven Gastauer for providing scattering model
717 software and advice. Also, we thank Jennifer Herbig for reading and editing an early draft of
718 the manuscript and for her statistical expertise. We acknowledge the valuable comments and
719 suggestions from the reviewers, which helped us to improve the quality of the manuscript.

720 **Author contribution statement**

721 MDu: Conceptualisation, Methodology, Software, Formal Analysis, Visualisation, Writing –
722 original draft

723 GP: Conceptualisation, Supervision, Writing – review & editing

724 SB: Investigation, Writing – review & editing

725 MDa: Conceptualisation, Investigation, Writing – review & editing

726 SFP: Investigation, Writing – review & editing

727 LC: Funding Acquisition, Resources

728 LB: Software, Visualisation

729 MG: Conceptualisation, Supervision, Writing – review & editing

730 **Funding statement**

731 This research was funded by GLIDER Phase I project, which was funded by the DEMO2000
732 research program (Norwegian Research Council and ConocoPhillips Skandinavia AS, project
733 no. 269188, "Unmanned ocean vehicles, a flexible and cost-efficient offshore monitoring and
734 data management approach") and by Glider Phase II financed by ConocoPhillips Skandinavia
735 AS. The research survey was funded by "Collaborative Studies of Two Resource Ecosystems in

736 Shelf, Slope and Oceanic Regions of the Norwegian and South China Seas (Stressor)", funded
737 by the Norwegian Research Council (project no. 287043). Maxime Geoffroy's participation is
738 financially supported by the Discovery Grant program of the Natural Science and Engineering
739 Research Council of Canada. Geir Pedersen's participation was co-funded by CRIMAC
740 (Norwegian Research Council project no. 309512).

741 **Competing interests**

742 The authors declare that they have no known competing financial interests or personal
743 relationships that could potentially influence the research reported in this paper.

744 **Data availability statement**

745 Acoustic data generated or analysed during this study are available in the "EK80 raw data
746 collected by autonomous sailbuoy in Lofoten/Vesterålen, 2018-06-18–2018-06-30"
747 repository (<https://doi.org/10.5281/zenodo.6786851>). Location and other sensor
748 observations from the autonomous surface vehicle data generated or analysed during this
749 study are available in the "Real-time oceanography captured by autonomous sailbuoy in
750 Lofoten/Vesterålen 2018" repository (<https://doi.org/10.5281/zenodo.6786919>)

751 **References**

- 752 Andersen, L.N., Chu, D., Heimvoll, H., Korneliussen, R., Macaulay, G.J. and Ona, E., 2021.
753 Quantitative processing of broadband data as implemented in a scientific splitbeam
754 echosounder. arXiv preprint arXiv:2104.07248. doi.org/10.1121/10.0002943
- 755 Anderson, C.I.H., Horne, J.K. and Boyle, J., 2007. Classifying multi-frequency fisheries acoustic
756 data using a robust probabilistic classification technique. *The Journal of the Acoustical Society*
757 *of America*, 121(6), pp.EL230-EL237. doi.org/10.1121/1.2731016
- 758 Appenzeller, A.R. and Leggett, W.C., 1992. Bias in hydroacoustic estimates of fish abundance
759 due to acoustic shadowing: evidence from day–night surveys of vertically migrating fish.
760 *Canadian Journal of Fisheries and Aquatic Sciences*, 49(10), pp.2179-2189.
761 doi.org/10.1139/f92-240
- 762 Bandara, K., Basedow, S.L., Pedersen, G. and Tverberg, V., 2022. Mid-summer vertical
763 behavior of a high-latitude oceanic zooplankton community. *Journal of Marine Systems*, 230,
764 p.103733. doi.org/10.1016/j.jmarsys.2022.103733
- 765 Barham, E.G., 1966. Deep scattering layer migration and composition: observations from a
766 diving saucer. *Science*, 151(3716), pp.1399-1403. doi.org/10.1126/science.151.3716.1399w,
- 767 S.L., Edvardsen, A. and Tande, K.S., 2006. Spatial patterns of surface blooms and recruitment
768 dynamics of *Calanus finmarchicus* in the NE Norwegian Sea. *Journal of plankton research*,
769 28(12), pp.1181-1190. doi.org/10.1093/plankt/fbl048
- 770 Basedow, S.L., McKee, D., Lefering, I., Gislason, A., Daase, M., Trudnowska, E., Egeland, E.S.,
771 Choquet, M. and Falk-Petersen, S., 2019. Remote sensing of zooplankton swarms. *Scientific*
772 *reports*, 9(1), pp.1-10. doi.org/10.1038/s41598-018-37129-x

773 Bassett, C., Lavery, A.C. and Stanton, T.K., 2019. Broadband measurements of the acoustic
774 target strength of mesopelagic fishes. *The Journal of the Acoustical Society of America*,
775 146(4), pp.2772-2772. doi.org/ 10.1121/1.5136601

776 Battaglia, A., Trenkel, V.M. and Rochet, M.J., 2006. Estimating end effects in trawl catches.
777 *ICES Journal of Marine Science*, 63(5), pp.956-959. doi.org/10.1016/j.icesjms.2006.03.002

778 Bellec, V., Wilson, M., Bøe, R., Rise, L., Thorsnes, T., Buhl-Mortensen, L. and Buhl-Mortensen,
779 P., 2008. Bottom currents interpreted from iceberg ploughmarks revealed by multibeam data
780 at Tromsøflaket, Barents Sea. *Marine Geology*, 249(3-4), pp.257-270.
781 doi.org/10.1016/j.margeo.2007.11.009

782 Benoit-Bird, K.J. and Waluk, C.M., 2020. Exploring the promise of broadband fisheries
783 echosounders for species discrimination with quantitative assessment of data processing
784 effects. *The Journal of the Acoustical Society of America*, 147(1), pp.411-427.
785 doi.org/10.1121/10.0000594

786 Benoit-Bird, K.J., 2009. The effects of scattering-layer composition, animal size, and numerical
787 density on the frequency response of volume backscatter. *ICES Journal of Marine Science*,
788 66(3), pp.582-593. doi.org/10.1093/icesjms/fsp013

789 Berge, J., Geoffroy, M., Daase, M., Cottier, F., Priou, P., Cohen, J.H., Johnsen, G., McKee, D.,
790 Kostakis, I., Renaud, P.E. and Vogedes, D., 2020. Artificial light during the polar night disrupts
791 Arctic fish and zooplankton behaviour down to 200 m depth. *Communications biology*, 3(1),
792 pp.1-8. doi.org/10.1038/s42003-020-0807-6

793 Blanluet, A., Doray, M., Berger, L., Romagnan, J.B., Le Bouffant, N., Lehuta, S. and Petitgas, P.,
794 2019. Characterisation of sound scattering layers in the Bay of Biscay using broadband

795 acoustics, nets and video. *PloS one*, 14(10), p.e0223618.
796 doi.org/10.1371/journal.pone.0223618

797 Branch, M. A., Coleman, T. F., & Li, Y. 1999. A subspace, interior, and conjugate gradient
798 method for large-scale bound-constrained minimisation problems. *SIAM Journal on Scientific*
799 *Computing*, 21(1), 1-23. doi.org/10.1137/s1064827595289108

800 Brinton, E., 1967. Vertical migration and avoidance capability of euphausiids in the California
801 Current. *Limnology and Oceanography*, 12(3), pp.451-483.
802 doi.org/10.4319/lo.1967.12.3.0451

803 Camus, L., Pedersen, G., Falk-Petersen, S., Dunlop, K., Daase, M., Basedow, S.L., Bandara, K.,
804 Tverberg, V., Pederick, J., Peddie, D. and Langeland, T., 2019. Autonomous surface and
805 underwater vehicles reveal new discoveries in the Arctic Ocean. *OCEANS 2019-Marseille*,
806 pp.1-8. doi.org/10.1109/oceanse.2019.8867089

807 Chu, D. and Wiebe, P.H., 2005. Measurements of sound-speed and density contrasts of
808 zooplankton in Antarctic waters. *ICES Journal of Marine Science*, 62(4), pp.818-831.

809 Chu, D., and Ye, Z. 1999. A phase-compensated distorted wave born approximation
810 representation of the bistatic scattering by weakly scattering objects: Application to
811 zooplankton. *The Journal of the Acoustical Society of America*, 106(4), 1732-1743.
812 doi.org/10.1016/j.icesjms.2004.12.020

813 Chu, D., Wiebe, P.H., Copley, N.J., Lawson, G.L. and Puvanendran, V., 2003. Material
814 properties of North Atlantic cod eggs and early-stage larvae and their influence on acoustic
815 scattering. *ICES Journal of Marine Science*, 60(3), pp.508-515. [doi.org/10.1016/s1054-](https://doi.org/10.1016/s1054-3139(03)00047-x)
816 [3139\(03\)00047-x](https://doi.org/10.1016/s1054-3139(03)00047-x)

817 Cotter, E., Bassett, C. and Lavery, A., 2021. Classification of broadband target spectra in the
818 mesopelagic using physics-informed machine learning. *The Journal of the Acoustical Society*
819 *of America*, 149(6), pp.3889-3901. [doi.org/10.1016/s1054-3139\(03\)00047-x](https://doi.org/10.1016/s1054-3139(03)00047-x)

820 Davison, P.C., Koslow, J.A. and Kloser, R.J., 2015. Acoustic biomass estimation of mesopelagic
821 fish: backscattering from individuals, populations, and communities. *ICES Journal of Marine*
822 *Science*, 72(5), pp.1413-1424. doi.org/10.1093/icesjms/fsv023

823 De Robertis, A., Wilson, C.D. and Williamson, N.J., 2012. Do silent ships see more fish?
824 Comparison of a noise-reduced and a conventional research vessel in Alaska. In *The Effects of*
825 *Noise on Aquatic Life* (pp. 331-334). Springer, New York, NY. [doi.org/10.1007/978-1-4419-](https://doi.org/10.1007/978-1-4419-7311-5_74)
826 [7311-5_74](https://doi.org/10.1007/978-1-4419-7311-5_74)

827 De Robertis, A., Lawrence-Slavas, N., Jenkins, R., Wangen, I., Mordy, C.W., Meinig, C., Levine,
828 M., Peacock, D. and Tabisola, H., 2019. Long-term measurements of fish backscatter from
829 Sairdrones unmanned surface vehicles and comparison with observations from a noise-
830 reduced research vessel. *ICES Journal of Marine Science*, 76(7), pp.2459-2470.
831 doi.org/10.1093/icesjms/fsz124

832 Demer, D.A. and Hewitt, R.P., 1995. Bias in acoustic biomass estimates of *Euphausia superba*
833 due to diel vertical migration. *Deep Sea Research Part I: Oceanographic Research Papers*,
834 42(4), pp.455-475. [doi.org/10.1016/0967-0637\(94\)e0005-c](https://doi.org/10.1016/0967-0637(94)e0005-c)

835 Demer, D.A., Berger, L., Bernasconi, M., Bethke, E., Boswell, K., Chu, D., Domokos, R.,
836 Dunford, A., Fassler, S., Gauthier, S. and Hufnagle, L.T., 2015. Calibration of acoustic
837 instruments. doi.org/10.23919/oceans40490.2019.8962778

838 Dietz, R.S., 1948. Deep scattering layer in the Pacific and Antarctic Oceans. *Journal of marine*
839 *research*, 7(3), pp.430-442.

840 Dornan, T., Fielding, S., Saunders R.A. and Genner, M.J., 2022. Large mesopelagic fish biomass
841 in the Southern Ocean resolved by acoustic properties. *Proceedings of the Royal Society B*,
842 289(1967), p.20211781. <https://doi.org/10.1098/rspb.2021.1781>

843 Elizondo, U.H. and Vogt, M., 2022. Individual-based modeling of shelled pteropods. *Ecological*
844 *Modelling*, 468, p.109944. doi.org/10.1016/j.ecolmodel.2022.109944

845 Falk-Petersen, S., Gatten, R.R., Sargent, J.R. and Hopkins, C.C.E., 1981. Ecological
846 investigations on the zooplankton community in Balsfjorden, Northern Norway: seasonal
847 changes in the lipid class composition of *Meganyctiphanes norvegica* (M. Sars), *Thysanoessa*
848 *raschii* (M. Sars), and *T. inermis* (Krøyer). *Journal of Experimental Marine Biology and*
849 *Ecology*, 54(3), pp.209-224. [doi.org/10.1016/0022-0981\(81\)90158-1](https://doi.org/10.1016/0022-0981(81)90158-1)

850 Falk-Petersen, S. and Kristensen, Å., 1985. Acoustic assessment of krill stocks in Ullsfjorden,
851 north Norway. *Sarsia*, 70(1), pp.83-90. doi.org/10.1080/00364827.1985.10420620

852 Feuillade, C. and Nero, R.W., 1998. A viscous-elastic swimbladder model for describing
853 enhanced-frequency resonance scattering from fish. *The Journal of the Acoustical Society of*
854 *America*, 103(6), pp.3245-3255. doi.org/10.1121/1.423076

855 Foote, K.G., 1983. Linearity of fisheries acoustics, with addition theorems. *The Journal of the*
856 *Acoustical Society of America*, 73(6), pp.1932-1940. doi.org/10.1121/1.389583

857 Gastauer, S., Chu, D. and Cox, M.J., 2019. ZooScatR—An r package for modelling the
858 scattering properties of weak scattering targets using the distorted wave Born

859 approximation. *The Journal of the Acoustical Society of America*, 145(1), pp.EL102-EL108.
860 doi.org/10.1121/1.5085655

861 Gjørseter, H., Ingvaldsen, R. and Christiansen, J.S., 2020. Acoustic scattering layers reveal a
862 faunal connection across the Fram Strait. *Progress in Oceanography*, 185, p.102348.
863 doi.org/10.1016/j.pocean.2020.102348

864 Greenlaw, C.F., 1979. Acoustical estimation of zooplankton populations 1. *Limnology and*
865 *Oceanography*, 24(2), pp.226-242. doi.org/10.4319/lo.1979.24.2.0226

866 Handegard, N.O. and Tjøstheim, D., 2005. When fish meet a trawling vessel: examining the
867 behaviour of gadoids using a free-floating buoy and acoustic split-beam tracking. *Canadian*
868 *Journal of Fisheries and Aquatic Sciences*, 62(10), pp.2409-2422. doi.org/10.1139/f05-131

869 Holliday, D.V., 1977. Extracting bio-physical information from the acoustic signature of
870 marine organisms. *Oceanic sound scattering prediction*, pp.619-624.

871 Holliday, D.V. and Pieper, R.E., 1995. Bioacoustical oceanography at high frequencies. *ICES*
872 *Journal of Marine Science*, 52(3-4), pp.279-296. [doi.org/10.1016/1054-3139\(95\)80044-1](https://doi.org/10.1016/1054-3139(95)80044-1)

873 Hetherington, E.D., Choy, C.A., Thuesen, E.V. and Haddock, S.H., 2022. Three Distinct Views of
874 Deep Pelagic Community Composition Based on Complementary Sampling Approaches.
875 *Frontiers in Marine Science*, 9. doi.org/10.3389/fmars.2022.864004

876 Jech, J.M., Horne, J.K., Chu, D., Demer, D.A., Francis, D.T., Gorska, N., Jones, B., Lavery, A.C.,
877 Stanton, T.K., Macaulay, G.J. and Reeder, D.B., 2015. Comparisons among ten models of
878 acoustic backscattering used in aquatic ecosystem research. *The Journal of the Acoustical*
879 *Society of America*, 138(6), pp.3742-3764. doi.org/10.1121/1.4937607

880 Kędra, M., Renaud, P.E. and Andrade, H., 2017. Epibenthic diversity and productivity on a
881 heavily trawled Barents Sea bank (Tromsøflaket). *Oceanologia*, 59(2), pp.93-101.
882 doi.org/10.1016/j.oceano.2016.12.001

883 Kieser, R., and Mulligan, T. J., 1984. Analysis of echo counting data: a model. *Canadian*
884 *Journal of Fisheries and Aquatic Sciences*, 41(3), pp.451-458. doi.org/10.1139/f84-054

885 Khodabandeloo, B., Agersted, M.D., Klevjer, T., Macaulay, G.J. and Melle, W., 2021.
886 Estimating target strength and physical characteristics of gas-bearing mesopelagic fish from
887 wideband in situ echoes using a viscous-elastic scattering model. *The Journal of the Acoustical*
888 *Society of America*, 149(1), pp.673-691. doi.org/10.1121/10.0003341

889 Knutsen, T., Wiebe, P.H., Gjørseter, H., Ingvaldsen, R.B. and Lien, G., 2017. High latitude
890 epipelagic and mesopelagic scattering layers—A reference for future Arctic ecosystem
891 change. *Frontiers in Marine Science*, 4, p.334. doi.org/10.3389/fmars.2017.00334

892 Kögeler, J.W., Falk-Petersen, S., Kristensen, Å., Pettersen, F. and Dalen, J., 1987. Density-and
893 sound speed contrasts in sub-Arctic zooplankton. *Polar Biology*, 7(4), pp.231-235.
894 doi.org/10.1007/bf00287419

895 Lavery, A.C., Wiebe, P.H., Stanton, T.K., Lawson, G.L., Benfield, M.C. and Copley, N., 2007.
896 Determining dominant scatterers of sound in mixed zooplankton populations. *The Journal of*
897 *the Acoustical Society of America*, 122(6), pp.3304-3326. doi.org/10.1121/1.2793613

898 Lavery, A.C., Chu, D. and Moum, J.N., 2010. Measurements of acoustic scattering from
899 zooplankton and oceanic microstructure using a broadband echosounder. *ICES Journal of*
900 *Marine Science*, 67(2), pp.379-394. doi.org/10.1093/icesjms/fsp242

901 Lee, W.J., Staneva, V., Mayorga, E., Nguyen, K., Satiawan, L. and Majeed, I., 2021. Echotype:
902 Enhancing the interoperability and scalability of ocean sonar data processing. *The Journal of*
903 *the Acoustical Society of America*, 149(4), pp.A63-A63. doi.org/10.1121/10.0004522

904 Love, R.H., 1975. Predictions of volume scattering strengths from biological trawl data. *The*
905 *Journal of the Acoustical Society of America*, 57(2), pp.300-306. doi.org/10.1121/1.380460

906 Liu, L.G., Chen, C.C., Lin, C.C. and Yang, Y.J., 2005. Elasticity of single-crystal aragonite by
907 Brillouin spectroscopy. *Physics and Chemistry of Minerals*, 32(2), pp.97-102.
908 doi.org/10.1007/s00269-005-0454-y

909 Lloyd, S., 1982. Least squares quantisation in PCM. *IEEE transactions on information theory*,
910 28(2), pp.129-137. doi.org/10.1109/tit.1982.1056489

911 Mordy, C.W., Cokelet, E.D., De Robertis, A., Jenkins, R., Kuhn, C.E., Lawrence-Slavas, N.,
912 Berchok, C.L., Crance, J.L., Sterling, J.T., Cross, J.N. and Stabeno, P.J., 2017. Advances in
913 ecosystem research: Sairdrone surveys of oceanography, fish, and marine mammals in the
914 Bering Sea. *Oceanography*, 30(2), pp.113-115. doi.org/10.5670/oceanog.2017.230

915 Moriarty, M., Sell, A.F., Trenkel, V.M., Lynam, C.P., Burns, F., Clarke, E.D., Greenstreet, S.P.R.
916 and McGonigle, C., 2018. Resolution of biodiversity and assemblage structure in demersal
917 fisheries surveys: the role of tow duration. *ICES Journal of Marine Science*, 75(5), pp.1672-
918 1681. doi.org/10.1093/icesjms/fsy050

919 Ohman, M.D., Davis, R.E., Sherman, J.T., Grindley, K.R., Whitmore, B.M., Nickels, C.F., and
920 Ellen, J.S., 2019. Zooglider: an autonomous vehicle for optical and acoustic sensing of
921 zooplankton. *Limnology and Oceanography: Methods*, 17(1), 69-86.
922 doi.org/10.1002/lom3.10301

923 Olsen, E., Aanes, S., Mehl, S., Holst, J. C., Aglen, A., & Gjøsæter, H. 2010. Cod, haddock, saithe,
924 herring, and capelin in the Barents Sea and adjacent waters: a review of the biological value
925 of the area. *ICES Journal of Marine Science*, 67(1), 87-101. doi.org/10.1093/icesjms/fsp229

926 Pearcy, W.G., Greenlaw, C.F. and Pommeranz, T., 1983. Assessment of euphausiids with five
927 nets and a 120-kHz echosounder in fjords of northern Norway. *Biological Oceanography*, 2(2-
928 4), pp.151-177. doi.org/10.1080/00364827.1968.10411128

929 Pedersen, G., Falk-Petersen, S., Dunlop, K., Camus, L., Daase, M., Basedow, S.L., Bandara, K.,
930 Tverberg, V., Pederick, J. and Peddie, D., 2019, June. Autonomous surface vehicles for
931 persistent acoustic monitoring of zooplankton in a highly productive shelf area. In *OCEANS*
932 *2019-Marseille*. pp. 1-7. IEEE. doi.org/10.1109/oceanse.2019.8867089

933 Peña, M., 2019. Mesopelagic fish avoidance from the vessel dynamic positioning system. *ICES*
934 *Journal of Marine Science*, 76(3), pp.734-742. doi.org/10.1093/icesjms/fsy157

935 Proud, R., Cox, M.J., Wotherspoon, S. and Brierley, A.S., 2015. A method for identifying sound
936 scattering layers and extracting key characteristics. *Methods in Ecology and Evolution*, 6(10),
937 pp.1190-1198. doi.org/10.1111/2041-210x.12396

938 Proud, R., Cox, M.J., Le Guen, C. and Brierley, A.S., 2018. Fine-scale depth structure of pelagic
939 communities throughout the global ocean based on acoustic sound scattering layers. *Marine*
940 *Ecology Progress Series*, 598, pp.35-48. doi.org/10.3354/meps12612

941 Reiss, C.S., Cossio, A.M., Walsh, J., Cutter, G.R. and Watters, G.M., 2021. Glider-Based
942 estimates of meso-zooplankton biomass density: a fisheries case study on antarctic krill
943 (*Euphausia superba*) around the northern antarctic peninsula. *Frontiers in Marine Science*, 8,
944 p.256. doi.org/10.3389/fmars.2021.604043

945 Rogers, A. D., 2015. Environmental change in the Deep Ocean. *Annual Review of Environment*
946 *and Resources*. 40(1), pp. 1–38. doi.org/10.1146/annurev-environ-102014-021415

947 Santana Hernández, N., 2019. *A patch of Calanus finmarchicus in the Lofoten-Vesterålen*
948 *Region. Characteristics and determining factors* (Master's thesis, UiT Norges arktiske
949 universitet).

950 Simmonds, J. and MacLennan, D.N., 2008. *Fisheries acoustics: theory and practice*. John Wiley
951 & Sons. doi.org/10.1002/9780470995303

952 Skjoldal, H.R., Wiebe, P.H., Postel, L., Knutsen, T., Kaartvedt, S. and Sameoto, D.D., 2013.
953 Intercomparison of zooplankton (net) sampling systems: Results from the ICES/GLOBEC sea-
954 going workshop. *Progress in oceanography*, 108, pp.1-42.
955 doi.org/10.1016/j.pocean.2012.10.006

956 Solvang, H.K., Haug, T., Knutsen, T., Gjørseter, H., Bogstad, B., Hartvedt, S., Øien, N. and
957 Lindstrøm, U., 2021. Distribution of rorquals and Atlantic cod in relation to their prey in the
958 Norwegian high Arctic. *Polar Biology*, 44(4), pp.761-782. doi.org/10.1007/s00300-021-02835-
959 2

960 Stanton, T.K., Chu, D., Wiebe, P.H., Eastwood, R.L. and Warren, J.D., 2000. Acoustic scattering
961 by benthic and planktonic shelled animals. *The Journal of the Acoustical Society of*
962 *America*, 108(2), pp.535-550. doi.org/10.1121/1.429584

963 Trevorrow, M.V., Mackas, D.L. and Benfield, M.C., 2005. Comparison of multifrequency
964 acoustic and in situ measurements of zooplankton abundances in Knight Inlet, British
965 Columbia. *The Journal of the Acoustical Society of America*, 117(6), pp.3574-3588.
966 doi.org/10.1121/1.1920087

967 Trudnowska, E., Gluchowska, M., Beszczynska-Möller, A., Blachowiak-Samolyk, K. and
968 Kwasniewski, S., 2016. Plankton patchiness in the Polar Front region of the West Spitsbergen
969 Shelf. *Marine Ecology Progress Series*, 560, pp.1-18. doi.org/10.3354/meps11925

970 Verfuss, U.K., Aniceto, A.S., Harris, D.V., Gillespie, D., Fielding, S., Jiménez, G., Johnston, P.,
971 Sinclair, R.R., Sivertsen, A., Solbø, S.A. and Storvold, R., 2019. A review of unmanned vehicles
972 for the detection and monitoring of marine fauna. *Marine pollution bulletin*, 140, pp.17-29.
973 doi.org/10.1016/j.marpolbul.2019.01.009

974 Wiebe, P.H., Boyd, S.H., Davis, B.M. and Cox, J.L., 1982. Avoidance of towed nets by the
975 euphausiid *Nematoscelis megalops* [Fish behavior]. *Fishery bulletin-United States, National*
976 *Marine Fisheries Service (USA)*.

977 Warren, J.D., Stanton, T.K., Wiebe, P.H. and Seim, H.E., 2003. Inference of biological and
978 physical parameters in an internal wave using multiple-frequency, acoustic-scattering data.
979 *ICES Journal of Marine Science*, 60(5), pp.1033-1046. [doi.org/10.1016/s1054-3139\(03\)00121-](https://doi.org/10.1016/s1054-3139(03)00121-8)
980 [8](https://doi.org/10.1016/s1054-3139(03)00121-8)

981 Whitmore, B.M., Nickels, C.F. and Ohman, M.D., 2019. A comparison between Zooglider and
982 shipboard net and acoustic mesozooplankton sensing systems. *Journal of Plankton Research*,
983 41(4), pp.521-533. doi.org/10.1093/plankt/fbz033